Edge collection function: an analytical expression for the optical efficiency of an energy-harvesting device based on photoluminescence

Ichiro Fujieda
Yasuhiro Tsutsumi
Kohei Yunoki
Yoshiki Yamada

SPIE.

Edge collection function: an analytical expression for the optical efficiency of an energy-harvesting device based on photoluminescence

Ichiro Fujieda,* Yasuhiro Tsutsumi, Kohei Yunoki, and Yoshiki Yamada
Ritsumenkan University, Department of Electrical and Electronic Engineering, Kusatsu, Shiga, Japan

Abstract. An edge collection function is proposed for characterizing the optical efficiency of an energy-harvesting system that utilizes photoluminescence (PL) in a waveguide. We assume that a single spot in a waveguide is excited and that PL is isotropic. For the photons to be collected by one edge of the waveguide, they must be emitted toward the edge, trapped in the waveguide and they must survive self-absorption on the way. The optical efficiency is formulated as the product of these probabilities. When this function is calculated for every spot on the waveguide and for each wavelength of the PL spectrum, the efficiency of the system is given by superposition. Its validity is checked by a Monte Carlo simulation for the case of no self-absorption loss. In experiment, we fabricate a 5-cm² waveguide with a thin layer of Lumogen F Red 305 and measure its efficiency by placing a photodiode array in the vicinity of its edge with a small air gap. The formula roughly reproduces the efficiency and its dependency on the position of the excitation spot. This analytical approach allows one to estimate the optical efficiency for an arbitrary incident light distribution with small computational complexity. © *The Authors. Published by SPIE under a Creative Commons Attribution 4.0 Unported License. Distribution or reproduction of this work in whole or in part requires full attribution of the original publication, including its DOI.* [DOI: [10.1117/1.OE.58.10.104101](https://doi.org/10.1117/1.OE.58.10.104101)]

1 Introduction

A luminescent solar concentrator (LSC) consists of a waveguide containing luminescent materials and solar cells attached to at least one of its edges.[1] The luminescent materials convert direct sunlight as well as ambient light to photoluminescence (PL) photons, and they propagate inside the waveguide by repeating total internal reflection (TIR). Those reaching the solar cells are harvested. A laser phosphor display displays an image by projecting intensity-modulated blue or ultraviolet light on a screen with phosphor regions.[2–4] Using an LSC as its screen, one can display an image while recovering a part of the laser power.[5] When the light source is turned off, the screen can generate power by harvesting ambient light. This energy-harvesting display might be incorporated in a wall, a window, and a billboard. The key parameter for such an energy-harvesting device is the optical efficiency with which the PL photons reach the solar cells. For example, due to the loss of PL photons during the waveguiding step, the highest power conversion efficiency of an LSC remains to be 7.1%, which was reported in 2008 for a 5×5 cm²-area device.[6]

The optical efficiency of an LSC is expressed by integral forms and is estimated by either numerical integration[1,7,8] or Monte Carlo simulation.[9,10] Both approaches assume that the incident photon distribution is uniform. This assumption is not valid for an energy-harvesting display. In addition, the computational complexity for numerical integration and Monte Carlo technique might hinder repetitive analysis required for optimizing design parameters.

The objective of this study is to provide an analytical expression that allows us to estimate the optical efficiency for an arbitrary incident light distribution. In Sec. 2, we introduce an "edge collection function (ECF)."[11] The validity of the model is checked by a Monte Carlo simulation for the case of no self-absorption loss. In Sec. 3, we describe an experiment with square fluorescent waveguides (FWGs) and show that this simple model roughly reproduces the measurement.

2 Theory

A point spread function (PSF) describes the response of an imaging system to a delta-function input. The response of the system for an arbitrary input is given by weighting, shifting, and superimposing PSFs. We can adopt this concept for the current problem of estimating the optical efficiency of an energy-harvesting device for an arbitrary incident photon flux distribution. We start by placing an isotropic emitter at a single point (x, y) in a square waveguide with a luminescent material. We call such a waveguide as an FWG in this paper. For simplicity, the light propagation is assumed to be one way: the other three edges absorb light and no reemission events occur. We also restrict our discussion at a particular wavelength λ for the moment. Suppose that the probability of collecting the photons from this emitter at one edge of an FWG is known for all (x, y). Let us call this probability an ECF and express it as $\mathrm{ECF}(x, y, \lambda)$. We also denote an arbitrary incident excitation photon flux at wavelength λ_ex as $I_\mathrm{in}(x, y, \lambda_\mathrm{ex})$. Then the PL photon flux collected by this edge is expressed as follows:

$$I_\mathrm{out}(\lambda) = \eta_\mathrm{QY} S_\mathrm{em}(\lambda) \iint \mathrm{ECF}(x, y, \lambda) I_\mathrm{in}(x, y, \lambda_\mathrm{ex}) \mathrm{d}x \mathrm{d}y, \quad (1)$$

*Address all correspondence to Ichiro Fujieda, E-mail: fujieda@se.ritsumei.ac.jp

where η_{QY} is the quantum yield of the luminescent material and $S_{em}(\lambda)$ is its emission spectrum.

In this section, we express $ECF(x, y, \lambda)$ for the bottom edge of the square waveguide. The ECFs for other edges is obtained by considering symmetry. In Sec. 2.1, any absorption losses during the light propagation are neglected. In Sec. 2.2, we take these into account by introducing an attenuation coefficient and invoke the Lambert–Beer law. Our model neglects scattering events and it can be applied for uniform luminescent materials such as organic dyes. Furthermore, we assume that the luminescent material is confined in a thin layer inside an FWG because a thick layer would blur the displayed images.

2.1 Model without Absorption Loss

2.1.1 Optical efficiency

As illustrated in Fig. 1(a), we place an isotropic emitter in a thin layer inside a square FWG at (X_0, Y_0). The light from this point source is trapped in the waveguide if the polar angle of its emission direction θ is between θ_c and $\pi - \theta_c$, where θ_c is the critical angle for TIR. This trapping probability is equal to $\cos \theta_c$ for an isotropic emitter.[1] Incidentally, the expression for a dipole emitter is a little more complicated.[12]

Let us consider the probability of the light reaching the section on the bottom edge from $x = x_i$ to $x_i + \Delta x$. In a two-dimensional space, this probability $\eta_{reach}(x_i)$ is equal to $\varphi_d/2\pi$, where φ_d is the angle subtended by this section. The incident angle φ_{in} and the angle φ_d are given by Eqs. (2) and (3), respectively. In a three-dimensional space, the light needs to be trapped in the waveguide. Hence $\eta_{reach}(x_i)$ is given by Eq. (4). The thickness of the FWG is denoted as ℓ as shown in Fig. 1(b):

$$\varphi_{in} = \left| \tan^{-1} \frac{X_0 - x_i}{Y_0} \right|, \tag{2}$$

$$\varphi_d = \left| \left| \tan^{-1} \frac{X_0 - x_i - \Delta x}{Y_0} \right| - \varphi_{in} \right|, \tag{3}$$

$$\eta_{reach}(x_i) = \frac{\varphi_d}{2\pi} \times \cos \theta_c. \tag{4}$$

For the trapped light to exit the FWG, we consider the reflectance of the light reaching the edge surface. This factor

R_F is given by the Fresnel equations.[13] Assuming that the waveguide is surrounded by air and denoting the index of refraction of the waveguide as n, R_F is given by the average of reflectance for the two polarization components as follows:

$$R_F(\varphi_{in}) = \frac{1}{2} \left\{ \left[\frac{\sin(\varphi_{in} - \varphi_r)}{\sin(\varphi_{in} + \varphi_r)} \right]^2 + \left[\frac{\tan(\varphi_{in} - \varphi_r)}{\tan(\varphi_{in} + \varphi_r)} \right]^2 \right\}, \tag{5}$$

where $\varphi_r = \sin^{-1}(n \sin \varphi_{in})$.

In addition, the trapped light needs to avoid TIR at the edge surface. For this, the propagation angle θ_p must be smaller than θ_c as illustrated in Fig. 1(b). In the case of $\theta_c < \frac{\pi}{4}$, this probability is given by the ratio of $\int_0^{\theta_c} \sin \theta d\theta$ and $\int_0^{\frac{\pi}{2} - \theta_c} \sin \theta d\theta$, which is equal to $1 - \cos \theta_c / 1 - \sin \theta_c$. Therefore, the probability of the light trapped in the waveguide to exit from the section $x_i \leq x \leq x_i + \Delta x$ is given by

$$\eta_{exit}(x_i) = \eta_{reach}(x_i) \times [1 - R_F(\varphi_{in})] \times \frac{1 - \cos \theta_c}{1 - \sin \theta_c}. \tag{6}$$

In the case of $\theta_c > \frac{\pi}{4}$, the last factor in Eq. (6) is replaced by $1 - \sin \theta_c / 1 - \cos \theta_c$.

As defined above, the ECF is the efficiency for collecting the light at one edge of a waveguide. The ECF for the light reaching the bottom edge is obtained by adding $\eta_{reach}(x_i)$. When the waveguide is surrounded by air, the ECF is obtained by adding $\eta_{exit}(x_i)$. In both cases, the ECF depends on the coordinates of the point source (X_0, Y_0):

$$ECF_k = \sum_i \eta_k(x_i), \qquad k = \text{reach or exit.} \tag{7}$$

Note that the analysis presented so far is essentially two-dimensional as apparent from the fact that the resultant probabilities and ECFs do not depend on the thickness of the waveguide ℓ. This is because we neglected the loss of light during propagation.

2.1.2 Numerical example

For example, we calculated the probability of reaching the bottom edge $\eta_{reach}(x_i)$ and the probability of exiting there $\eta_{exit}(x_i)$ for a 50 mm $\times$ 50 mm FWG with refractive index
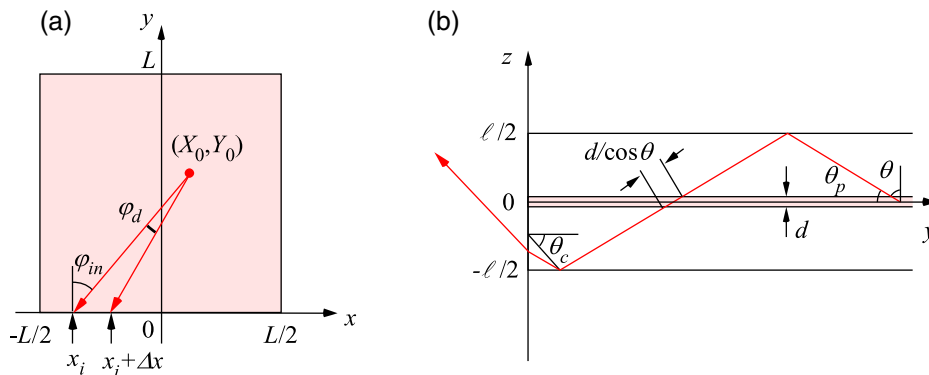
Fig. 1 Trajectories of the light from an isotropic point source placed at a single spot in a rectangular parallelepiped waveguide. The probabilities of the light reaching and exiting the waveguide in the xz plane are expressed as a function of the coordinate of the point source: (a) top view and (b) cross section.

of 1.5. Its 50 mm-long bottom edge was divided into 128 sections and the source position was moved on the y axis in increments of 5 mm in this example. The probability distribution $\eta_{\text{reach}}(x_i)$ is shown in Fig. 2(a). As the point source moves toward the bottom edge, the distribution in Fig. 2(a) becomes taller and narrower. The probability distribution $\eta_{\text{exit}}(x_i)$ is shown in Fig. 2(b). It becomes zero at the position where the TIR condition is met at the bottom edge. The abrupt change of the probability close to this position is due to the sharp increase in R_F.

The ECFs were calculated for this waveguide by dividing its incident area into 1000×1000 rectangular regions and placing a point source at each grid point. Each point in the color-coded images in Fig. 3 represents the ECF corresponding to the position of the point source (X_0, Y_0). The column at the right end in each image is the color scale normalized by the maximum value in each case. The curves show the dependency of the ECF on Y_0 for some selected values of X_0. As shown in Fig. 3(a), the ECF for the light reaching the bottom edge decreases monotonically with increasing Y_0. The ECFs for the other three edges are obtained by rotating these ECFs. By adding the resultant ECFs, the probability of collecting the light at the four edges is given. The result (not shown) is equal to $\cos \theta_c$, and it no longer depends on the location of the point source. The ECF for the light exiting the waveguide from the bottom edge is shown in Fig. 3(b). In contrast to Fig. 3(a), it remains constant until Y_0 exceeds a certain threshold value (about 30 mm for the case of $X_0 = 0.25$ mm). This behavior is explained by considering an isosceles triangle with an apex angle of $2\theta_c$. As long as the bottom edge fully covers the bottom section of this triangle, the ECF is constant. As the source moves away from the bottom edge or toward the right or left edge of the waveguide, the bottom section of the triangle becomes only partially covered by the bottom edge and the ECF decreases. However, even with the 1000×1000 grid adopted in this calculation, the data for $Y_0 \leq 3$ mm are slightly overestimated due to the quantization error in estimating the factor $\varphi_d/2\pi$

in Eq. (4). With the coarser grid of 100×100, this error range extended to $Y_0 \leq 10$ mm.[11]

### 2.1.3 Comparison to Monte Carlo simulation

The simple model described above is not three dimensional (3-D). To check its validity, we carried out a 3-D Monte Carlo simulation. Using a commercial software LightTools from Synopsys, Inc, the geometry shown in Fig. 1 was modeled in a 3-D space: an isotropic monochromatic light source was placed on a single spot on the surface of a 50 mm $\times$ 50 mm transparent plate with refractive index of 1.5. Its thickness was set to either 4 mm or 10 mm. A detector of 50×10 rectangular regions was placed in the vicinity of one edge surface with a small air gap to record the rays exiting the plate. The other three edges were assumed to be absorbing. We moved the point source on the y axis with increments of 5 mm. Radiance distributions for each case are compared in Fig. 4(a). Each color-coded image represents the radiance distribution for a corresponding y coordinate of the point source (Y_0) and the scale at the right end is normalized by the maximum radiance for each plate. The ECFs are extracted from these color-coded images by adding all the values and dividing by the optical power generated by the source. The result is plotted in Fig. 4(b). Also plotted and denoted as "simple model" is the ECF at $X_0 = 0.25$ mm for $Y_0 \geq 3$ mm in Fig. 3(b).

As shown in Fig. 4(a), the radiance distribution for the 4-mm-thick plate is more or less uniform along the thickness direction. The 10 mm-thick plate exhibits nonuniformity especially when the point source is placed near the edge. The top three images for this plate reveal that the profile along the thickness direction oscillates with Y_0. This behavior is caused by the reflectance R_F, which varies sharply near the critical angle for TIR. In both cases, the distributions spread out as the point source moves away from the edge.

As shown in Fig. 4(b), the two curves from the Monte Carlo simulation coincide almost completely, indicating that there is no dependency on the plate thickness. This is
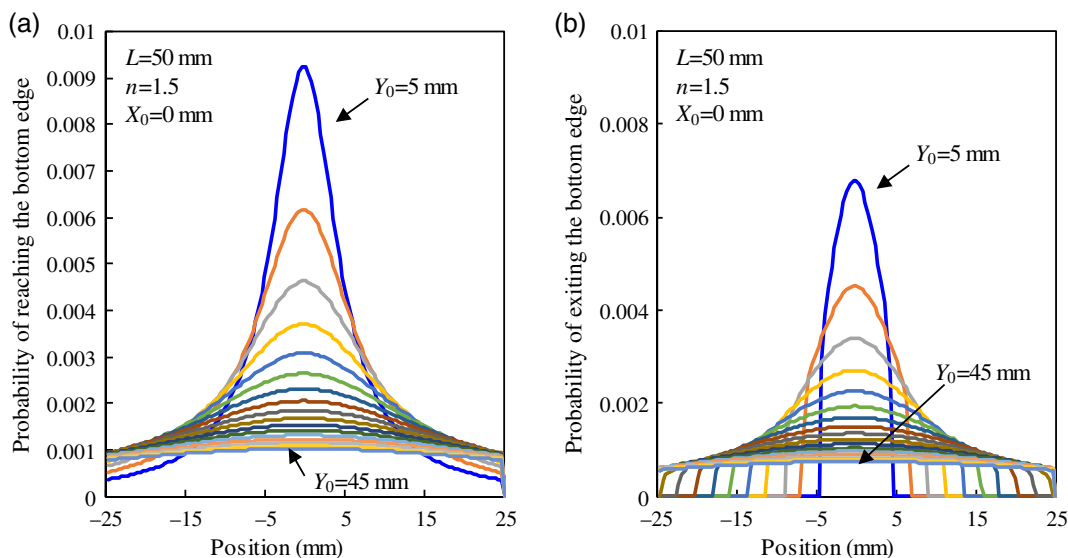
Fig. 2 Numerical example for the probability of the light (a) reaching and (b) exiting the bottom edge surface. The isotropic point source is assumed to be at (X_0, Y_0) in a 50 mm $\times$ 50 mm FWG with refractive index of 1.5.
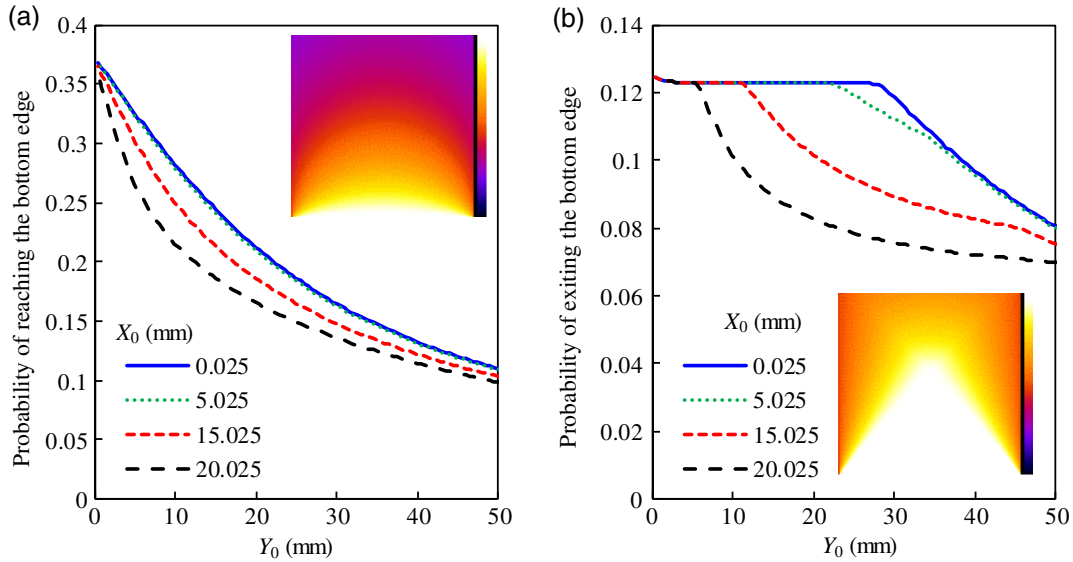
Fig. 3 ECF for the example in Fig. 2: (a) the ECF for the light reaching the bottom edge and (b) the ECF for the light exiting the waveguide from its bottom edge.
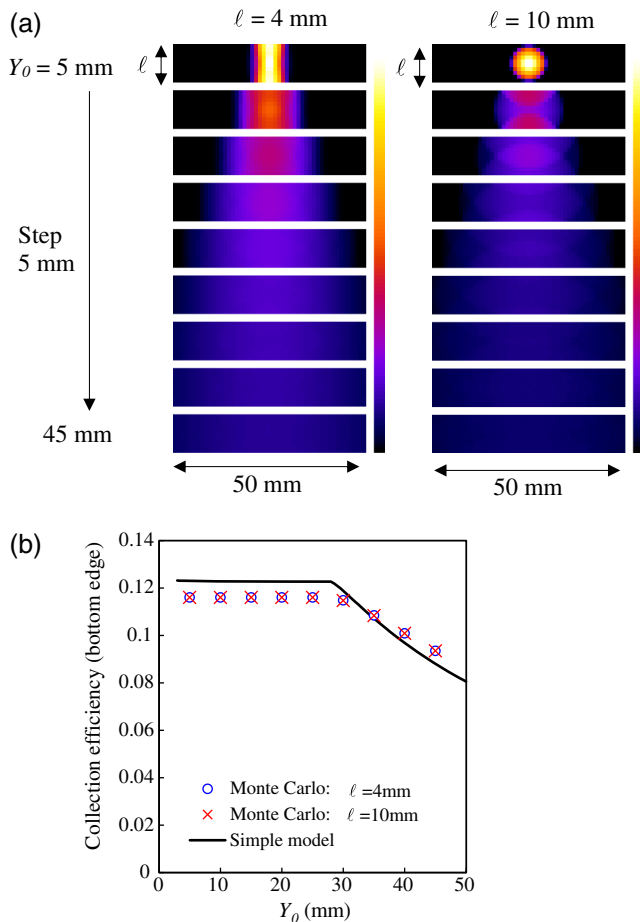
Fig. 4 Radiance distributions obtained by a 3-D Monte Carlo simulation for the monochromatic light exiting the bottom edge. The point source is moved on the y axis with increments of 5 mm: (a) comparison of the distributions for a 4-mm-thick plate and those for a 10-mm-thick plate and (b) the ECFs obtained by the Monte Carlo simulation and the simple analytical model are compared.

because optical losses during propagation are neglected. The simple model reproduces the 3-D Monte Carlo simulation reasonably well. The discrepancy between them might be caused by the fact that the model is only quasi-2-D.

2.2 Model Incorporating Absorption Loss

2.2.1 Optical efficiency

To account for absorption loss in an FWG, we invoke Lambert–Beer law with a linear attenuation coefficient $\mu(\lambda)$. Let us consider the light propagating with a polar angle θ as shown in Fig. 1(b). The total distance that this light traverses the luminescent layer before reaching the bottom edge at $x = x_i$ is approximated as follows:

$$
\begin{aligned}
s &\approx \frac{d}{\cos\theta} \times \frac{\sqrt{(X_0 - x_i)^2 + Y_0^2}}{\ell \tan\theta} \\
&= \frac{d}{\ell} \times \frac{1}{\sin\theta} \times \sqrt{(X_0 - x_i)^2 + Y_0^2}.
\end{aligned}
\tag{8}
$$

For an isotropic emitter, the average value of s is obtained by integrating Eq. (8) by θ from $\theta = \theta_c$ to $\pi/2$ and dividing the result by $\pi/2 - \theta_c$. The result is expressed as follows:

$$
\bar{s} = \frac{d}{\ell} \times \frac{2 \log\left|\tan\frac{\theta_c}{2}\right|}{\pi - 2\theta_c} \times \sqrt{(X_0 - x_i)^2 + Y_0^2}.
\tag{9}
$$

Let us define a new parameter μ_0 by Eq. (10). The linear attenuation coefficient $\mu(\lambda)$ is a material parameter while μ_0 contains design parameters in terms of d, ℓ, and θ_c. The two probabilities are rewritten as follows for the case of $\theta_c < \frac{\pi}{4}$, and the ECFs are modified accordingly:

$$
\mu_0 = \mu(\lambda) \times \frac{d}{\ell} \times \frac{2 \log\left|\tan\frac{\theta_c}{2}\right|}{\pi - 2\theta_c},
\tag{10}
$$

$$\eta_{\text{reach}}(x_i) = \frac{\varphi_d}{2\pi} \times \cos\theta_c \times \exp[-\mu_0\sqrt{(X_0 - x_i)^2 + Y_0^2}],$$

$$\text{(11)}$$

$$\eta_{\text{exit}}(x_i) = \eta_{\text{reach}}(x_i) \times [1 - R_F(\varphi_{\text{in}})] \times \frac{1 - \cos\theta_c}{1 - \sin\theta_c}. \quad (12)$$

2.2.2 Numerical example

First, we consider a weakly absorbing case. The ECFs calculated with $\mu_0 = 0.01$ mm^{-1} are shown in Fig. 5. The ECFs in Fig. 5(a) have smaller values than those in Fig. 3(a). The effect of attenuation during propagation is more apparent in the ECF curve for $X_0 = 0.25$ mm in Fig. 5(b): it decreases almost linearly with Y_0, whereas the corresponding curve in Fig. 3(b) is almost constant for $Y_0 < 30$ mm.

Next, we have repeated the calculation for the case of $\mu_0 = 0.1$ mm^{-1}. As shown in Fig. 6, the ECFs have substantially smaller values than those in Fig. 5. For example, the curve for $X_0 = 0.25$ mm in Fig. 6(b) is well fit by an exponential function and the $1/e$ distance is about 9 mm. Hence, only the light emitted in the peripheral region of the waveguide is harvested under this condition.

2.3 Extension of the Model

In the discussion on the function $\text{ECF}(x, y, \lambda)$ so far, the wavelength λ was fixed. A real device involves a number of photons generated by excitation photons at a single spot in an FWG. For handling these photons with longer wavelengths, we extend our model below.

The parameter μ_0 defined by Eq. (10) is a function of the wavelength via the material parameter $\mu(\lambda)$. Let us set the parameter μ_0 equal to the absorption coefficient of an FWG at each wavelength. If we neglect re-emission events and denote the spectrum of the luminescent material as $S_{\text{em}}(\lambda)$, the probability of collecting these photons by one edge is given by simply weighting $\text{ECF}(x, y, \lambda)$ with $S_{\text{em}}(\lambda)$. Naming this probability as total edge collection function (TECF), it is expressed as follows:

$$\text{TECF}_k(x, y) = \int S_{\text{em}}(\lambda) \times \text{ECF}_k(x, y, \lambda) \mathrm{d}\lambda,$$

$$\text{(13)}$$

$$k = \text{reach or exit.}$$

Let us consider an example of an organic dye, Lumogen F Red 305. We took its absorbance and emission data from the literature,[14] converted the absorbance to absorption coefficient, and normalized the two spectra by their respective peak values. The result is shown in Fig. 7(a). Although the wavelength resolution can be set as fine as desired, we consider only three ranges to illustrate the procedure of this analysis. Photons in range I and II are strongly and weakly absorbed by the dye, respectively. The boundary between them is somewhat arbitrary. There is no absorption for the photons in range III. The proportion of the photons emitted in each range is given by integrating $S_{\text{em}}(\lambda)$. The result is 0.026 (range I), 0.420 (range II), and 0.554 (range III). For this illustration purpose, we calculate the TECF using these weighting factors and the three ECFs in the numerical examples described above. As shown in Fig. 7(b), the TECF is dominated by the ECFs in ranges II and III.

The model described so far is limited to the optical efficiency of an FWG excited by a monochromatic light. We can extend it to calculate the photocurrent as follows. The photon flux collected by one edge of the FWG is given as a function of the wavelength by Eq. (1). By multiplying it with the quantum efficiency of a solar cell $\eta_{\text{sc}}(\lambda)$ and integrating by the wavelength, the number of electrons generated per unit time is given. Denoting the elementary charge as q_e, the photocurrent I_{photo} is expressed as follows. For this calculation, the integration by the wavelength is performed on the product of $S_{\text{em}}(\lambda)$, $\text{ECF}_k(x, y, \lambda)$, and $\eta_{\text{sc}}(\lambda)$:

$$I_{\text{photo}} = q_e \int \eta_{\text{sc}}(\lambda) \times I_{\text{out}}(\lambda) \mathrm{d}\lambda. \quad (14)$$

Following the modeling steps described above, important design parameters for enhancing the optical efficiency are
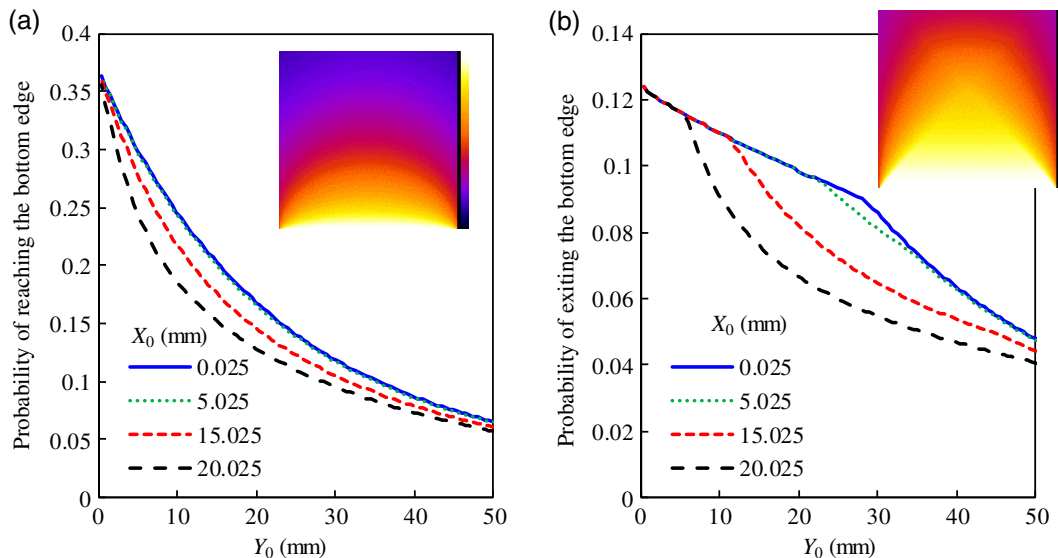
Fig. 5 ECFs for a weakly absorbing case ($\mu_0 = 0.01$ mm^{-1}): (a) the ECF for the light reaching the bottom edge and (b) the ECF for the light exiting the waveguide from its bottom edge.
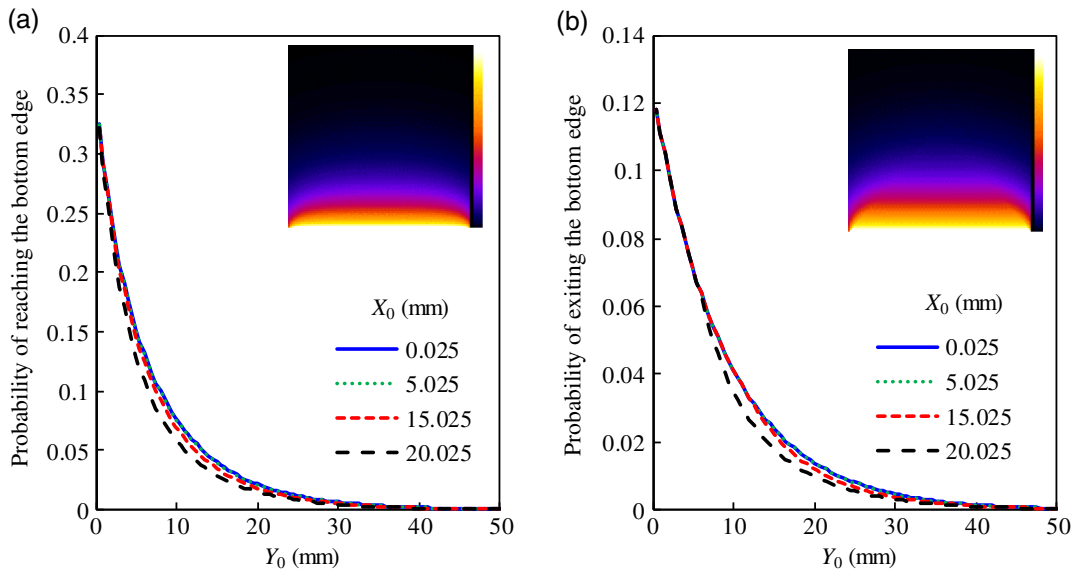
Fig. 6 ECFs for a strongly absorbing case ($\mu_0 = 0.1$ mm^{-1}): (a) the ECF for the light reaching the bottom edge and (b) the ECF for the light exiting the waveguide from its bottom edge.
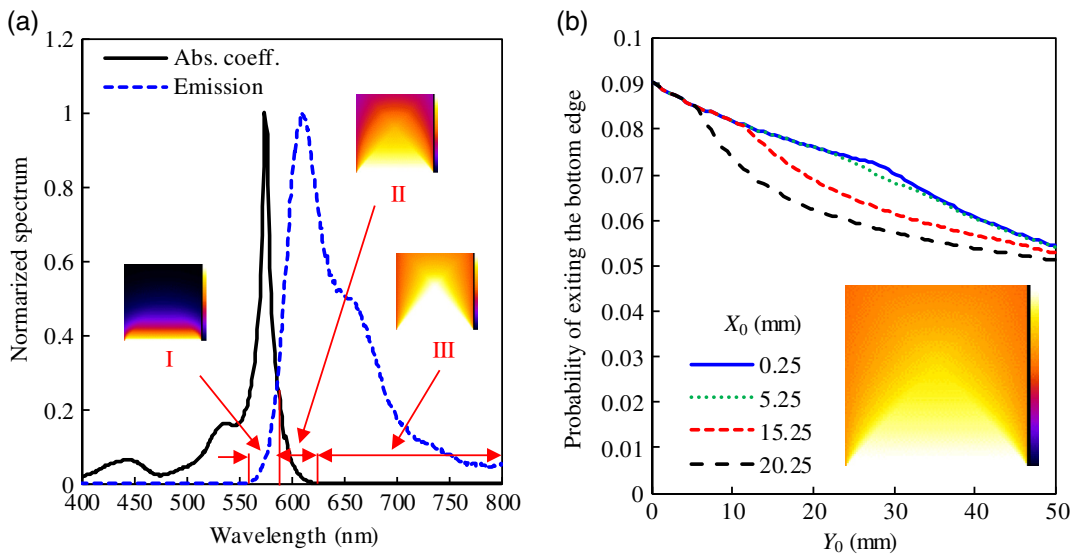
Fig. 7 A TECF is roughly calculated by dividing the emission spectrum into three wavelength ranges and weighting a representative ECF in each range by the proportion of the photons within its range. (a) Normalized absorption coefficient and emission spectrum of Lumogen F Red 305. (b) The inset image is the resultant TECF and the curves are the TECFs along the specified x coordinates (X_0).

identified. The ECF is proportional to the product of the quantum yield of the luminescent material and three probabilities: the probability of the PL photons being emitted toward the edge, the probability of being trapped in the waveguide via TIR, and the probability of surviving self-absorption on the way to the edge. The first probability is determined purely geometrically if the emission is isotropic. Because the second probability is equal to $\cos \theta_c$ for an isotropic emitter, the refractive index of the waveguide is an important parameter. The third probability is determined by the emission spectrum $S_{em}(\lambda)$, the absorption coefficient $\mu(\lambda)$, and the thickness of the waveguide ℓ. Hence, these parameters need to be set carefully to mitigate self-absorption.

3 Experiment

3.1 *Method*

A single spot on an FWG is excited by a laser beam and the power of the light exiting its bottom edge is measured with a photodiode (PD) array.[15] The procedure of this experiment is as follows. An FWG is fabricated by mixing organic dye (BASF, Lumogen F Red 305) and ultraviolet curable resin (Norland Products, NOA81), sandwiching the mixture with two 50 mm × 50 mm acrylic plates and curing the resin. It is reported that the Lumogen dyes have near 100% quantum yields.[16] The PD array (Hamamatsu Photonics K.K., S11865) has 128 PDs and the sensitive area of each PD is 0.3 mm × 0.6 mm. It is placed in the vicinity of the edge

in this experiment because butt-coupling to the edge of an FWG with an index-matching oil tends to damage the bonding-wires of the PD array. The small air gap in between results in a complication to be discussed below. The other three edges of the FWG are painted black. A laser emitting at 450 nm (Z-Laser, Z20M18H-F450pe) is used and its spot size is about 0.1 mm. We measure the spectrum of the light exiting the edge of an FWG with a spectrometer (Ocean Optics, FLAME-S) and calibrate the PD array with a power meter (Ophir, PD300-SH). The incident position of the laser beam on the y axis is varied in increments of 5 mm. We repeat this measurement with multiple FWGs with thicknesses ranging from 2 to 6 mm.

3.2 Result

The PD array outputs obtained with a 6-mm-thick FWG and a 2-mm-thick FWG are compared in Fig. 8. We adjusted the incident power of the laser light such that the two FWGs generate a comparable signal. It was 121 μW for the 6-mm-thick FWG and 49.8 μW for the 2-mm-thick FWG. The transmittance of these FWGs at 450 nm varied from 0.92 to 0.96. The thinner FWG generated a larger signal per unit excitation power due to the higher geometrical concentration. Also apparent is the shift of the baseline in these distributions. This is caused by the light exiting the bottom edge, propagating in the air gap, and landing on the PDs. This baseline shift is larger for the 6-mm-thick FWG because each PD faces a larger light-emitting surface in the thickness direction as schematically shown in the insets. Although reflection at the other three edge surfaces of an FWG could raise the baseline, our measurement on reflectance of the black paint used in the experiment shows that it is unlikely.

3.3 Analysis

By adding the PD output and scaling the result by the ratio of the area of the edge surface and the sensitive area of the PDs, we estimate the total optical power exiting the edge surface. Dividing this value by the incident optical power gives the
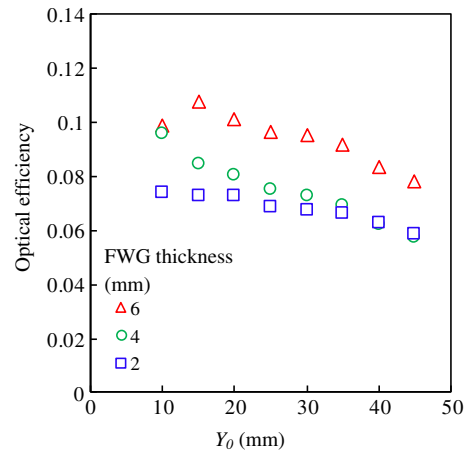
Fig. 9 Optical efficiency for collecting light at the bottom edge of an FWG. The excitation spot was moved on the y axis in the coordinate system defined in Fig. 1(a). As the spot moves away from the edge, the efficiency decreases.

optical efficiency for collecting the light from the excited spot. The scaling by the areal ratio is valid if the optical power exiting the edge surface is uniform. We show this efficiency for the three FWGs in Fig. 9.

The result in Fig. 9 indicates that the model roughly reproduces the value of the efficiency and its dependency on the position of the excitation spot. Namely, the efficiency of the 6-mm-thick FWG decreases from about 0.1 as the y coordinate of the excitation spot (Y_0) increases. This behavior resembles to the curve for $X_0 = 0.25$ mm in Fig. 7(b). The efficiency of the thinner FWGs in Fig. 9 is lower, suggesting that they have larger attenuation coefficients. This is consistent to the fact that the light crosses the luminescent layer more often before it reaches the edge in a thinner FWG. The efficiency of the 4-mm-thick FWG become almost equal to that for the 2-mm-thick FWG for $Y_0 \geq 40$ mm, suggesting that self-absorption is completed in this range of Y_0. The datum at $Y_0 = 10$ mm for the
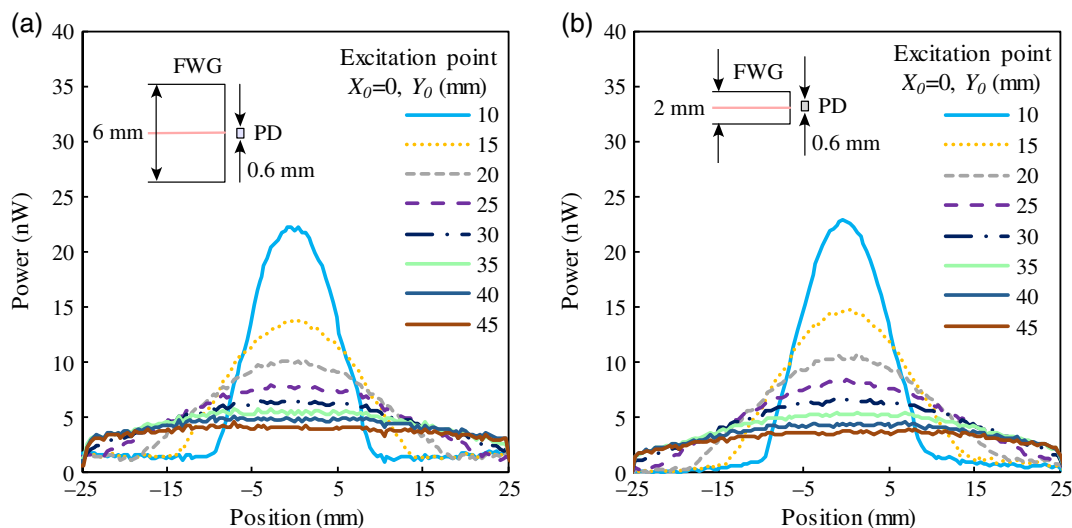
Fig. 8 Intensity distributions measured by the PD array placed in the vicinity of the bottom edge: (a) 6-mm-thick FWG and (b) 2-mm-thick FWG. The incident power was 121 μW for the 6-mm-thick FWG and 49.8 μW for the 2-mm-thick FWG. The inset in each graph shows the cross section of a PD facing the edge surface of the FWG.

6-mm-thick FWG is an exception. When the excitation spot moves closer to the edge, the intensity distribution becomes nonuniform as shown in Fig. 4(b). Hence, the scaling by the areal ratio leads to an erroneous value. This is especially the case for a thicker FWG, which requires a longer lateral distance for making the intensity distribution at the edge homogenous.

4 Conclusion

Conventional approaches for analyzing the optical efficiency of an LSC are based on either numerical integration or Monte Carlo simulation. They assume that the incident radiation pattern is uniform. This is not true for the case of an energy-harvesting display where a modulated excitation light is projected on an LSC to display an image. For handling an arbitrary pattern, we introduce an ECF. This is defined as the probability of collecting the photons by one edge of an FWG when a narrow beam of light excites a single spot on the waveguide. Hence, this is a function of the coordinates of the excitation spot. We start this analysis by placing an isotropic emitter at a single spot in a square waveguide. The ECF is proportional to the product of the following factors: the quantum yield of the luminescent material, the probability of the photons being emitted toward the edge, the probability of being trapped in the waveguide, and the probability of surviving self-absorption on the way to the edge. This function is calculated for every spot on the waveguide and for each wavelength of the PL spectrum. Then in analogous to the PSF for an imaging system, the response of a system for an arbitrary incident pattern can be calculated by superimposing this function. To check its validity for the case of no self-absorption loss, we carried out a Monte Carlo simulation. The ECFs generated by the two methods coincided reasonably well. In experiment, we fabricated a 5-cm^2 waveguide with a thin layer of Lumogen F Red 305. Its optical efficiency was measured by placing a PD array in the vicinity of its edge with a small air gap and exciting a single spot with a narrow laser beam. For example, the efficiency of a 6-mm-thick sample decreased from about 0.1 as the excited spot moved away from the edge. The model roughly reproduced this dependency on the coordinates of the excitation spot. Because its computational burden is light, the model might be useful for an initial design of energy-harvesting devices utilizing luminescent materials.

References

1. W. H. Weber and J. Lambe, "Luminescent greenhouse collector for solar radiation," *Appl. Opt.* **15**(10), 2299–2300 (1976).
2. R. A. Hajjar, "Introducing scalable, freeform, immersive, high-definition laser phosphor displays," *SID Dig.* **43**, 985–988 (2012).
3. R. A. Hajjar, "Seamless scalable large format display," *SID Dig.* **49**, 737–739 (2018).
4. T. X. Sun et al., "A novel emissive projection display (EPD) on fully-transparent phosphor screen," *SID Dig.* **50**, 394–397 (2019).
5. I. Fujieda et al., "Energy-harvesting laser phosphor display and its design considerations," *J. Photonics Energy* **7**(2), 028001 (2017).
6. L. H. Slooff et al., "A luminescent solar concentrator with 7.1% power conversion efficiency," *Phys. Status Solidi RRL* **2**(6), 257–259 (2008).
7. J. S. Batchelder, A. H. Zewai, and T. Cole, "Luminescent solar concentrators. 1: theory of operation and techniques for performance evaluation," *Appl. Opt.* **18**(18), 3090–3110 (1979).
8. V. I. Klimov et al., "Quality factor of luminescent solar concentrators and practical concentration limits attainable with semiconductor quantum dots," *ACS Photonics* **3**, 1138–1148 (2016).
9. R. W. Olson, R. F. Loring, and M. D. Fayer, "Luminescent solar concentrators and the reabsorption problem," *Appl. Opt.* **20**(17), 2934–2940 (1981).
10. J. Sansregret et al., "Light transport in planar luminescent solar concentrators: the role of DCM self-absorption," *Appl. Opt.* **22**(4), 573–577 (1983).
11. I. Fujieda et al., "Simple analytical model for optical efficiency of an energy-harvesting projector," *Proc. SPIE* **11120**, 111200H (2019).
12. C. L. Mulder et al., "Dye alignment in luminescent solar concentrators: I. Vertical alignment for improved waveguide coupling," *Opt. Express* **18**, A79–A90 (2010).
13. E. Hecht, *Optics*, 4th ed., p. 113, Addison Wesley, San Francisco (2002).
14. L. Desmet et al., "Monocrystalline silicon photovoltaic luminescent solar concentrator with 4.2% power conversion efficiency," *Opt. Lett.* **37**, 3087–3089 (2012).
15. I. Fujieda et al., "Measurement of optical power recovered by planar fluorescent waveguides for single-spot excitation," in *Proc. 25th Int. Display Workshops*, pp. 494–497 (2018).
16. L. R. Wilson and B. S. Richards, "Measurement method for photoluminescent quantum yields of fluorescent organic dyes in polymethyl methacrylate for luminescent solar concentrators," *Appl. Opt.* **48**(2), 212–220 (2009).

Ichiro Fujieda received his PhD from the University of California, Berkeley, in 1990. He was at Xerox Palo Alto Research Center from 1990 to 1992 and NEC Corporation from 1992 to 2003 before joining Ritsumeikan University in 2003.

Yasuhiro Tsutsumi received his BE, ME, and PhD degrees from Osaka Prefecture University in 2007, 2009, and 2012, respectively. He is an assistant professor at Ritsumeikan University. His current research interests include optical sensing, optical fiber devices, and optical communications.

Kohei Yunoki has been working on measurements and ray tracing simulations for an energy-harvesting projector since December 2017. He started his graduate studies at Ritsumeikan University in April 2019.

Yoshiki Yamada has been working on optical efficiency measurements of fluorescent waveguides since December 2017. He started his graduate studies at Ritsumeikan University in April 2019.